DEPARTMENT OF TRANSPORTATION

A Mechanistic Design Approach for Graphite Nanoplatelet (GNP) Reinforced Asphalt Mixtures for Low Temperature Applications

Jia-Liang Le, Principal Investigator
Department of Civil, Environmental, and Geo- Engineering
University of Minnesota

January 2018

Research Project
Final Report 2018-02

To request this document in an alternative format, such as braille or large print, call 651-366-4718 or 1-800-657-3774 (Greater Minnesota) or email your request to ADArequest.dot@state.mn.us. Please request at least one week in advance.

Technical Report Documentation Page

1. Report No.	2.	3. Recipients Accession No.
MN/RC 2018-02		

4. Title and Subtitle	5. Report Date
A Mechanistic Design Approach for Graphite Nanoplatelet (GNP) Reinforced Asphalt Mixtures for Low-Temperature Applications	January 2018
	6.

7. Author(s)	8. Performing Organization Report No.
Jia-Liang Le, Mihai Marasteanu, Rebecca Hendrickson	

9. Performing Organization Name and Address	10. Project/Task/Work Unit No.
Department of Civil, Environmental, and Geo- Engineering University of Minnesota 500 Pillsbury Dr., S.E. Minneapolis, MN, 55455.	2016014
	11. Contract (C) or Grant (G) No. (c) 99008 (wo) 186

12. Sponsoring Organization Name and Address	13. Type of Report and Period Covered
Minnesota Department of Transportation Research Services & Library 395 John Ireland Boulevard, MS 330 St. Paul, Minnesota 55155-1899	Final Report
	14. Sponsoring Agency Code

15. Supplementary Notes

http:// mndot.gov/research/reports/2018/201802.pdf

16. Abstract (Limit: 250 words)

This report explores the application of a discrete computational model for predicting the fracture behavior of asphalt mixtures at low temperatures based on the results of simple laboratory experiments. In this discrete element model, coarse aggregates are explicitly represented by spheres, and these spheres are connected by bonds representing the fine aggregate mixture, a.k.a. FAM, (i.e. asphalt binder with the fine-size aggregates). A literature review examines various methods of computational modeling of asphalt materials, as well as the application of nanomaterials to asphalt materials. Bending beam rheometer (BBR) tests are performed to obtain the mechanical properties of the fine aggregate mixture (FAM) at low temperatures. The computational model is then used to simulate the semi-circular bend (SCB) tests of the mixtures. This study considers both the conventional asphalt materials and graphite nanoplatelet (GNP) reinforced asphalt materials. The comparison between the simulated and experimental results on SCB tests shows that by employing a softening constitutive model of the FAM the discrete element model is capable of predicting the entire load-deflection curve of the SCB specimens. Based on the dimensional analysis, a parametric study is performed to understand the influence of properties of FAM on the predicted behavior of SCB specimens.

17. Document Analysis/Descriptors	18. Availability Statement
Fine aggregates, Asphalt mixtures, Pavement cracking, Simulation, Aggregates by shape and surface texture	No restrictions. Document available from: National Technical Information Services, Alexandria, Virginia 22312

19. Security Class (this report)	20. Security Class (this page)	21. No. of Pages	22. Price
Unclassified	Unclassified	50	

A MECHANISTIC DESIGN APPROACH FOR GRAPHITE NANOPLATELET (GNP) REINFORCED ASPHALT MIXTURES FOR LOW TEMPERATURE APPLICATIONS

FINAL REPORT

Prepared by:
Jia-Liang Le
Mihai Marasteanu
Rebecca Hendrickson
Department of Civil, Environmental, and Geo- Engineering
University of Minnesota

January 2018

Published by:
Minnesota Department of Transportation
Research Services & Library
395 John Ireland Boulevard, MS 330
St. Paul, Minnesota 55155-1899

TABLE OF CONTENTS

LIST OF FIGURES

LIST OF TABLES

EXECUTIVE SUMMARY

This report explores the application of a discrete computational model (PFC3D) for predicting the fracture behavior of asphalt mixtures at low temperatures based on the results of simple laboratory experiments. In this discrete element model, coarse aggregates are explicitly represented by spheres, and these spheres are connected by bonds representing the fine aggregate mixture, a.k.a. FAM, (i.e. asphalt binder with the fine-size aggregates). A literature review examines various methods of computational modeling of asphalt materials, as well as the application of nanomaterials to asphalt materials. Bending beam rheometer (BBR) tests are performed to obtain the mechanical properties of the fine aggregate mixture (FAM) at low temperatures. The computational model is then used to simulate the semi-circular bend (SCB) tests of the mixtures. This study considers both conventional asphalt materials and graphite nanoplatelet (GNP) reinforced asphalt materials. The comparison between the simulated and experimental results on SCB tests shows that by employing a softening constitutive model of the FAM the discrete element model is capable of predicting the entire load-deflection curve of the SCB specimens. Based on the dimensional analysis, a parametric study is performed to understand the influence of properties of FAM on the predicted behavior of SCB specimens.

CHAPTER 1: INTRODUCTION

Low-temperature cracking in asphalt pavements is a widespread concern especially in the northern states. Such failures could significantly shorten the lifespan and affect the durability of the pavements, which usually lead to costly pavement repair and rehabilitation [1]. Over decades, there has been a sustained amount of effort devoted toward improving the performance of asphalt pavements. A major part of these efforts has been focused on the development of new asphalt-based pavement materials, in which asphalt binders are modified by various additives including polymers, nano-clay, nano-silica, carbon nanotubes, basalt fibers, and graphite nano-platelets [2, 3, 4, 5, 6]. Extensive laboratory experiments are required to understand the influence of these additives on the fracture behavior of asphalt mixtures. One potential means of reducing the experimental efforts is to rely on computational models to predict the fracture behavior of the mixtures based on the properties of asphalt binders that could be measured by simple laboratory experiments.

In this study, we explore the application of a discrete element model for simulating the fracture behavior of asphalt mixtures at low temperatures. In this model, only the coarse aggregates are modeled explicitly as random-sized particles to improve the computational efficiency. The fine aggregates and asphalt binder are combined as fine aggregate mixtures (FAM), which are represented by the bonds between the coarse aggregates. The current discrete element model requires only the essential material properties of the FAM. By contrast, models that explicitly model the binder, aggregates and aggregate interfaces would require the knowledge of properties of all the constituents of the mixture. Meanwhile, inclusion of an excessive number of fine aggregates makes the computation practically unaffordable. The mechanical properties of FAM are measured using bending beam rheometer (BBR) tests, based on which the discrete element model is used to predict the peak load for the fracture behavior of the asphalt mixtures. Since the input parameters can be obtained from BBR experiments on FAM, we will be able to reduce the need for costly fracture experiments for determining the peak load capacity of the asphalt mixture. Though the bond fracture energy is used as a fitting parameter to determine the post-peak behavior, recommendations are provided on how to determine the bond fracture energy using simple BBR tests. It is noted that this research focuses on the low-temperature behavior of the asphalt mixtures. Therefore, the viscoelastic response is ignored since the asphalt mixtures exhibit brittle behavior at low temperatures.

The report is planned as follows: Section 2 provides a summary of previous literature; Section 3 describes the discrete element model; Section 4 presents the preparation of the samples, the BBR test of the FAM and semi-circular bend (SCB) test of the mixtures; Section 5 presents the comparison between the simulation results and the experimental observations and a parametric study on how the parameters of the discrete element model would influence the mixture behavior, and Chapter 6 presents a final discussion on the analysis presented in this report.

CHAPTER 2: LITERATURE REVIEW

The application of nanotechnology for asphalt mixtures has shown many benefits. Various nanomaterials have been used to evaluate the performance of modified asphalt, specifically for resistance to cracking and other forms of failure. In a recent study at the University of Minnesota, researchers developed graphite nanoplatelet (GNP) reinforced asphalt binders and mixtures, which exhibit a significant improvement in mechanical properties at low temperatures. However, there is currently not a comprehensive approach for determining the optimum mix design of the GNP reinforced asphalt binders and mixtures.

Although experimental test methods are indispensable for gaining insight into the behavior of nanomaterial-reinforced asphalt materials, these tests are usually very costly and time consuming, which makes them not ideal for identifying the optimum mix design. The use of computational modeling alongside lab results provides further understanding of the various physical mechanisms responsible for the observed behavior of the asphalt mixtures. The combination of computational and experimental investigations is advantageous for performing parametric studies to obtain the relationship between the mix design and the mechanical properties of asphalt mixtures with a minimum amount of laboratory testing.

In this section, we summarize the current efforts on the applications of nanotechnology to asphalt mixtures and their performance. In addition, we also discuss the two main computational methods that have been used for modeling the mechanical behavior of asphalt materials, namely the continuum approach and the discrete element method.

2.1 NANOMATERIALS

In recent years, there has been an emerging interest in applying nanotechnology to asphalt pavement materials. It was postulated that nanotechnology could potentially play a major role in the improved use of existing and available materials in pavements and in the material processing to improve the sustainability and resilience of the pavement [1]. Nanoparticles are commonly defined as particles with the least dimension being less than 100 nanometers [7]. Research has suggested that nanoclay, nanosilica, carbon nanotubes, basalt fibers and GNPs could lead to an improvement of the performance of the asphalt mixtures.

2.1.1 Nanoclays

Nanoclays are nanoparticles of layered mineral silicates. While being a naturally occur- ring inorganic material, nanoclay can be altered in order to make it compatible with organic monomers and polymers and has a layer thickness on the order of one nanometer [7, 8]. Compared to polymer-modified binder, nanoclays are relatively inexpensive since they are naturally occurring [9]. Not only are nanoclays a more cost-efficient option, they also have favorable mechanical properties such as their nanoscopic size and surface area which have shown tendencies for increasing stiffness of asphalt binders [5].

Extensive research has been focused on the use of nanoclays to reinforce asphalt binders. Although some types of nanoclay did not affect the stiffness or viscosity of the bitumen, other types of nanoclay did show encouraging results [3]. Upon testing stiffness and tensile strength, tensile modulus, flexural strength and modulus thermal stability, it was found that, compared to unmodified bitumen, the elasticity increased for the nanoclay-modified bitumen while the dissipation of mechanical energy was lower [3, 10]. Bentonite clay (BT) and organically modified bentonite (OBT) were also used to reinforce asphalt binders in pavement mixtures. While analyzed under shearing stresses and sonication, the modified asphalts ultimately had a higher rutting resistance, which could improve the low temperature rheological properties of asphalt [3, 11].

In order to gain a better understanding into the benefits of nanoclay modified binders, the nanostructure and microstructure as well as the mechanical behavior of asphalt clay nanocomposites has been investigated. Many atomic force microscopy (AFM) techniques were employed including tapping mode imaging, force spectroscopy and nanoindentation as well as X-ray diffraction (XRD) experiments. These techniques indicated that nanoclay had an exfoliated structure with enhanced adhesive forces [12]. Specific nanoscale properties like the state of dispersion and the exfoliation of the nanoclay binders have also been analyzed using techniques such as scanning electron microscopy (SEM) and (XRD) approaches [5]. Fourier transform infrared (FTIR) testing has also been employed to evaluate the interactions between nanoclay and asphalt [13]. The investigation of the nanoscale properties of the binders indicated that the improvement of the stiffness and hardness of the asphalt would depend on the temperature and percentage of nanoclay. These improvements appeared to be a result of the network of exfoliated nanoclay layers and the aggregates [12]. In general, the improvement of mechanical properties of the asphalt mixture can be better understood by studying the interactions of the aggregates and binders at a nanoscopic scale.

Recent studies on nanoclay-modified binders also showed an increase in the Superpave rutting factor and the rotational viscosity (RV) tests indicated a significant in- crease in viscosity. These results pointed toward nanoclay as an alternative to polymer-modified binders for more cost-efficient pavement solutions and maintenance [5]. Meanwhile, dynamic mechanical analysis, flexural creep stiffness and flexural tests on nanoclay-modified binders indicted that the temperature susceptibility and complex modulus in- crease while the phase angle decrease [13]. Other laboratory methods including the surface free energy (SFE) and small angle X-ray diffraction (SACD) techniques have been applied to nanoclay-modified asphalt mixtures to investigate the moisture susceptibility properties of nanoclay-modified asphalt binders [9]. Among its other benefits, nanoclay has also been found to improve the aging resistance and storage-ability of asphalt mixtures [9, 14]

2.1.2 **Nanosilica**

Silica is an abundant compound that has applications outside of material science in areas such as medication and drug distribution [3, 15]. Nanosilica has been used to reinforce elastomers as a rheological solute. Similar to nanoclay, nanosilica is an attractive option due to its low cost of production and high performance [3]. Laboratory testing has found a slight decrease in viscosity values with the addition of nanosilica in asphalt. This indicates that the compaction temperatures would be lower or lower energy of the construction process can be achieved [3]. It was found that the addition of nanosilica could enhance

anti-aging, fatigue cracking and rutting resistance and anti-stripping properties. Although beneficial in some aspects, the low temperature performance of nanosilica in asphalt binders was not remarkable. The stress relaxation capacity remained the same for nanosilica modified asphalt binders and in general, the low temperature properties of the asphalt binders were not greatly affected [3, 16].

Techniques used to analyze nanosilica-enhanced binders include morphological, rheological and thermal analysis techniques. Differential scanning calorimetry (DSC), thermogravimetric analysis (TGA), atomic force microscopy, and Fourier Transform Infrared spectroscopy (FTIR) were also used to quantify the effect of nanosilica as a binder modifier. The optimum content of the nanosilica modifier could be determined based primarily on the results from dynamic shear rheometer (DSR) asphalt fatigue and rutting tests [7]. Moisture susceptibility, resilient modulus, and dynamic creep tests were also employed to evaluate the performance of nanosilica particles added to polymer modified asphalt mixtures under different aging and moisture susceptibility conditions [17]. Scanning electron microscopy was used to analyze how well the particle dispersed into the asphalt binder. It was found that nanosilica could reduce the susceptibility to moisture damage and increase the strength as well as enhances the fatigue and rutting resistance of asphalt binders [17]. Additional laboratory tests include rotational viscosity (RV), bending beam rheometer (BBR), and flow number (FN) tests showing signs of an improved dynamic modulus, flow number and improved rutting and fatigue performance [17]. The results indicated that nanosilica produces beneficial results for asphalt pavement materials but does not specifically improve these materials under cold temperature conditions.

2.1.3 **Carbon Nanotubes**

Carbon nanotubes (CNT) are one-atom thin sheets of graphite shaped into a hollow cylinder [3]. Their diameter is on the order of one nanometer and CNTs have superior mechanical properties with high tensile strength [3]. Although there is less available literature for the use of CNTs to reinforce asphalt binders, improvements have been documented. Most prominently investigated in two forms, single and double wall nanotubes have been analyzed using atomic force microscopy. When adding CNTs to asphalt, an increase in adhesive forces has been noted as well as an increase in moisture susceptibility [18]. The morphology of CNT-modified hot mix asphalt was also examined using scanning electron microscopy. The mechanical properties, including resilient modulus, creep behavior, and fatigue performance indicated that CNTs produced an improvement against fatigue and permanent deformation compared to conventional HMA [6]. Overall, CNTs have produced results to indicate enhanced rutting resistance potential and enhanced resistance to thermal cracking [3]. However, it was found that the dispersion of CNTs in asphalt binders is a major challenge [19]. In order to achieve a good dispersion, the CNTs have to be added with some particular types of asphalt emulsions. With the relatively high material cost, the application of CNTs in asphalt pavements is rather limited.

2.1.4 **Basalt Fibers**

Basalt fiber is a material made from fine fibers of basalt, resembling carbon fiber and fiberglass. It is highly resistant to alkaline and salt creating potential use for concrete, bridge and shoreline structures [20]. Dynamic shear rheological tests and creep tests indicated that basalt fibers could lead to an improvement in the performance of asphalt binders [4]. Basalt fiber reinforced asphalt mixtures have demonstrated a high absorption ratio, low water absorption ratio and high tensile strength and temperature stability [4]. Fatigue properties of asphalt mixtures under complicated environment situations like low temperature

bending performance, chloride penetration, freezing-thawing cycle and their coupling effects were studied for basalt fiber reinforced asphalt mixtures [21]. The optimum dosage of basalt fiber was determined using the Marshall test and the results indicated that the tensile strength, the maximum curving tensile stress, the curving stiffness modulus, and fatigue properties are influenced by the chloride erosion and freezing-thawing cycle [21]. Therefore, low- temperature bending performance and fatigue properties of asphalt mixtures could be improved by adding moderate amounts of basalt fibers. The tensile strength of basalt fiber asphalt binder showed improvement using the results from the direct tension test [2]. Experimental results also indicated an overall improved low-temperature cracking resistance of asphalt concrete [22].

2.1.5 Graphite Nanoplatelets

Recent efforts have also been directed to the application of the graphite nanoplatelets (GNPs) to asphalt binders and mixtures. The GNPs are produced from the exfoliated graphite (Figure 2.1), which has shown great mechanical and electron transport proper- ties: the stiffness of graphite is on the order of 1 TPa, the strength of graphite is about 100 times that of steel, and the electric conductivity of graphite is somewhat higher than that of copper [23, 24, 25]. Furthermore, it has been shown that graphite has an exceptional thermal stability up to at least 2600K [26].

Recent studies have shown that, compared to CNTs, it is much easier to disperse the GNPs into asphalt binders. Due to its relatively low aspect ratio, no potential clustering was observed during the mixing. The complex shear modulus test indicated that the addition of GNP into both the polymer-modified and unmodified asphalt binders almost does not affect the complex shear modulus and phase angle. Strength tests showed that the GNP-modified asphalt binders exhibit superior flexural strength at low temperatures compared to conventional asphalt binders. For both polymer-modified and unmodified asphalt binders, a moderate addition of GNP, i.e. 3% to 6% by weight of the binder, can lead to about 130% increase in flexural strength. Meanwhile, it was also observed that the addition of GNP could lead to an increase in the indirect tensile strength and fracture energy of asphalt mixtures. Compared to the increase in flexural strength of GNP-modified asphalt binders, this increase is less significant. The addition of GNP can effectively reduce the compaction effort of the asphalt mixtures, and meanwhile it can also improve the rutting performance of the mixtures.

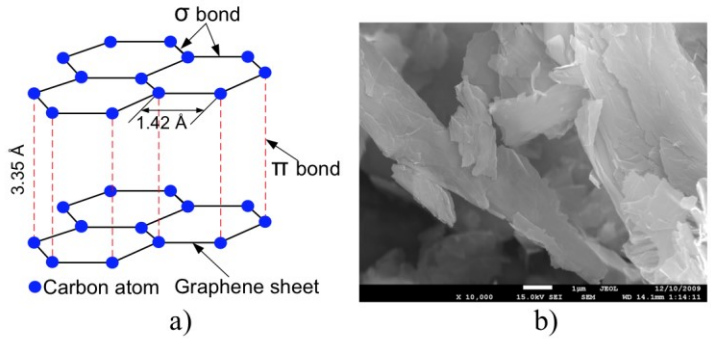

Figure 2.1: a) schematic of atomic structure of GNP, and b) SEM image of GNP

2.2 COMPUTATIONAL MODELS

Although experimental investigations provide a direct means of understanding of the mechanical properties of the nanomaterials and their interactions with asphalt mixtures, computational methods are particularly useful for predicting the behavior of asphalt binders and mixtures. The predictive models are valuable because they can reduce the costly experiments. To some extent, these models will allow us to perform experiments on computers, which are usually referred to as the simulation-based experiments. This concept has been developed for the design of various modern engineering structures, which experimental cost is prohibitively high. However, it has not been fully utilized for the mix design of asphalt mixtures.

The existing computational methods can be classified into two categories, which include the continuum approach and the discrete element method. The continuum approach provides efficient means of simulating the mechanical behavior of the asphalt mixtures, as it essentially smears the material inhomogeneity. By contrast, the discrete element method explicitly models the microstructure of the asphalt mixtures, which provides a more physical representation of the material, at the expense of a substantial higher requirement of the computational effort.

2.2.1 Finite Element Analysis

Many existing computational modeling of asphalt mixtures are essentially anchored by the use of the finite element (FE) approach. The FE method basically finds an approximate solution to the partial differential equations governing the boundary value problem, which could contain complex geometries. The essence of FE simulations is to incorporate a realistic constitutive model for asphalt mixtures. In a recent study [27], a continuum-damage model was proposed to determine internal state variables that can be used to predict the locally averaged amount of damage in an asphalt sample. Figure 2.2 shows how this model can be used to represent the overall locally averaged amount of damage to the asphalt sample where the individual aggregates are not modeled explicitly. Since the parameters are determined from testing specific samples, the continuum-damage mechanics model is specific to the type of mixture [28]. This approach takes into account the heterogeneous geometric characteristics and inelastic mechanical behavior of asphalt mixtures. With such a constitutive model, the FE model has been used to predict the damage and fracture of asphalt mixtures [28]. FEM can also incorporate the rate-dependent fracture failure properties alongside related experimental protocols. This model could help reduce experimental cost and time by achieving better insight into the properties of asphalt mixtures [29]. Beyond predicting failure in asphalt mixtures, the FE method has also been applied to model other physical processes, such as the progressive moisture damage behavior of asphalt [30]. Moisture damage due to water transport was incorporated with mechanical loading to simulate the nonlinear damage in the model. FEM could allow various parametric analyses to investigate how each of the parameters affects the moisture damage of that material [30].

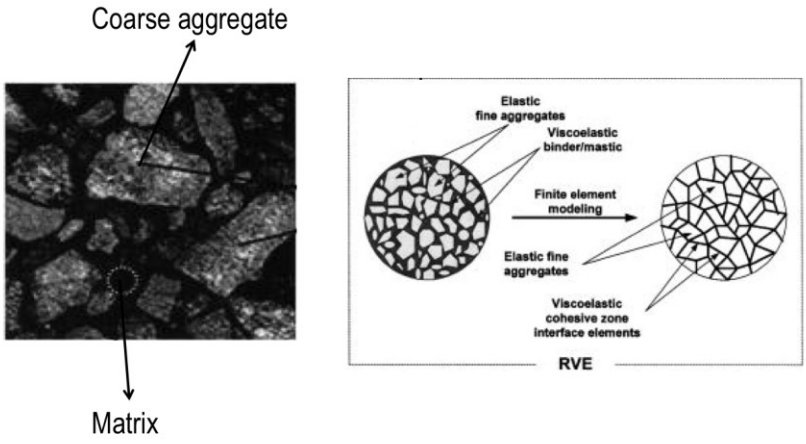

Figure 2.2: A typical asphalt concrete mixture is displayed with its finite element model representation [27].

The FE model essentially takes a smeared damage approach, which does not explicitly model the discrete fracture behavior. To better model the material fracture, the cohesive zone fracture model (CZM) has been often used within the framework of FE analysis. The CZM was pioneered for ductile and brittle fracture in the 1960s [31, 32], and was later extended to quasibrittle fracture [24, 33]. The essential idea of CZM is that it uses a nonlinear element to represent the fracture process zone at the crack tip, where the other part of the structure is treated as linearly elastic. Figure 2.3 demonstrates how the discrete cracks can be modeled by cohesive zones [28]. Figure 2.3 also shows the use of the cohesive zone model to represent the damage of the mixture [27]. The mechanical properties of the cohesive elements can be determined from the standard fracture tests in the laboratory. Compared to the smeared FE model, the CZM model is more efficient since the majority of the structure is modeled by elastic elements. Clearly the main drawback of the CZM is that the crack paths need to pre-determined in order to locate the cohesive elements. The CZM has been utilized to model the crack associated fracture damage in asphalt mixtures and can predict its performance under both nonlinear viscoelastic and fracture [28]. In a recent study, the CZM was used to investigate asphalts behavior due to fracture damage from repeated heavy truckloads [34].

Another continuum approach, which has recently attracted substantial attention, is the phase-field method. This method uses a parameter to describe the diffused damage around a discrete macro-crack, in which an intrinsic length scale is involved. The formulation of the method was anchored by the minimization of the potential energy of the structure, which leads to an efficient computation of fracture behavior. While classical fracture mechanics has been widely used to analyze initiation and propagation of cracks in asphalt, the phase field method has been more recently introduced for analyzing dynamic fracture. This method was used as a computational tool for analyzing Mode I cracking failure in asphalt binder using an energy-based formulation [1]. However, the existing formulation of the phase-field method was largely developed for linear elastic systems [35, 36], which has a limited applicability to asphalt mixtures.

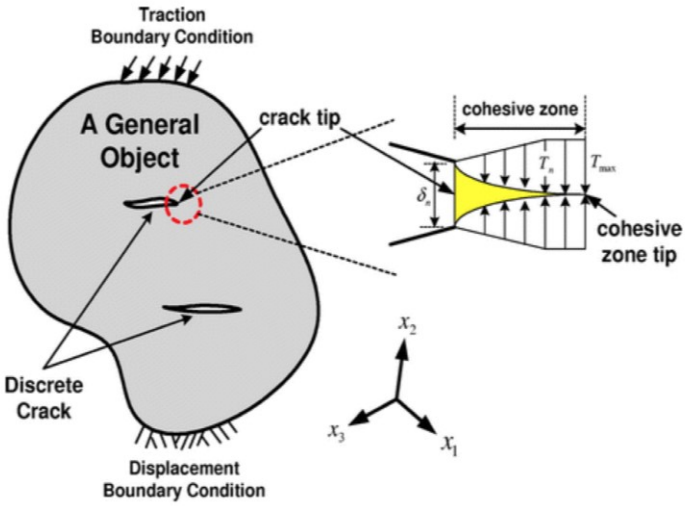

Figure 2.3: Schematic representation of cohesive zone concept for Mode-I fracture [37].

2.2.2 Discrete Element Modeling

As mentioned earlier, the continuum approach has its advantages for simplifying the analysis of asphalt mixtures through a smeared approach. By contrast, the discrete element model is designed to capture the details of the microstructure of the material. The model creates a more realistic alternative by taking into account the various size distributions of the aggregates [37, 38]. The discrete element model was pioneered by Cundall and Strack in the 1970s for modeling the behavior of large rock masses [39]. It has recently been applied to rock mechanics to simulate the tool-rock interaction process (cutting or indentation of rock depending on direction of the cut). The model was further applied to concrete materials [37, 40, 41, 42]. In this analysis, the rock mass was considered as an assembly of particles that can displace independently from one another [29]. This allows the DEM to model damage and brittle fracture of the bonds due to the particles ability to move independently of each other [37]. Similar to the analysis of asphalt mixtures, an understanding of the relationship between the large-scale solid material and the smaller scale group of aggregates is necessary in order to utilize the DEM.

In recent years, there has been a considerable amount of interests in applying discrete element models to asphalt mixtures [43, 44]. Studies have shown that, compared to the continuum-based finite element models, the discrete models could more realistically capture the underlying physics of the failure mechanism by explicitly taking into account the size distribution of the aggregates (Fig. 2.4). One main obstacles of using discrete element model is the excessive computational time especially if one wants to explicitly include fine aggregates. Meanwhile, the mechanical properties of the bonds are usually calibrated to fit some experiments on the mixture specimens [43]. Significant effort is required to accurately represent the microstructure of the mixture by utilizing image processing techniques [43, 44]. Although these models are able to capture the microstructure of asphalt mixtures by explicitly modeling the aggregates, binder and interface as clumps particles with unique parameters, these models require a number of model parameters [43]. There have been very few investigations on physically determining the mechanical behavior of the contacts between the particles [44]. In addition, such detailed modeling of the

asphalt mixture structure also requires significant computational time.

It is evident that the continuum-based finite element model is not suitable for the aforementioned purpose because the constitutive model must be calibrated for the entire mixture. Although more efficient than smeared FE models, methods like the cohesive zone model has been utilized to model the crack associated fracture damage in asphalt mixtures and can predict its performance under both nonlinear viscoelastic and fracture, these models require a pre-determined crack path in order to locate the cohesive elements [45]. By contrast, discrete computational models fit well for the above-mentioned predictions since they model the aggregates and binders separately. One important feature of the discrete element model is that it involves some characteristic length (e.g. particle size), which acts as a localization limiter regularizing the fracture energy.

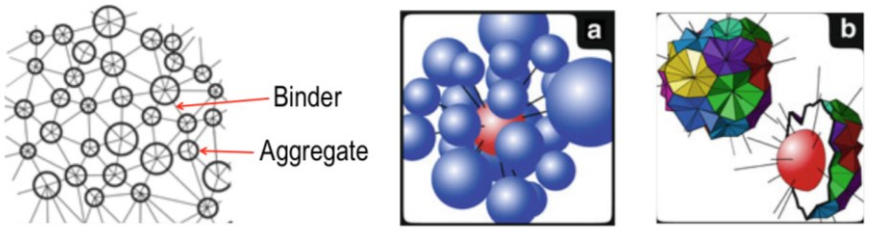

Figure 2.4: DEM representation of asphalt mixtures.

CHAPTER 3: DISCRETE ELEMENT COMPUTATIONAL MODEL

This section presents the discrete element computational model developed in this research. Section 3.1 describes the model and behavior of the bonded particles. Section 3.2 discusses the mixture material parameters that are used in the model, and Section 3.3 presents the input parameters, which represent the bond material properties.

3.1 MODEL DESCRIPTION

In this study, we adopt a commercially available discrete element software (PFC3D) [46]. The PFC3D model was developed based on the bonded-particle model (BPM) introduced by Potyondy and Cundall (2004). The model was initially used for simulation of the behavior of rock, which can be considered as a cemented granular material with varying shaped grains. The BPM has been used as a reliable computational tool to explore the micromechanics that produces macroscopic behaviors, and to predict the macroscopic behaviors of the rock.

The BPM allows for finite displacements and rotations of discrete bodies, simulating the mechanical behavior of bonded non-uniform sized spherical rigid particles [47]. The rigid particles interact at soft contacts which possess finite normal and shear stiffnesses and the mechanical behavior is described by the force and moment at each contact due to the movement of the particles. When the bond between particles is formed, the force and moment are initialed to zero. As external forces are applied, Newton's second law is used to determine the rotation and translation of the particles. The force-displacement law updates the contact forces that come from the relative motion of each particle at its contact point. The dynamic equilibrium equation is handled by a time-stepping algorithm where the time step is so small that disturbances would not spread farther than to the particle immediately next to it. To realistically capture the dynamic behavior, a damping force is applied to each particle to dissipate the kinetic energy [47].

In this study, we divide the aggregates into two categories, namely coarse aggregates and fine aggregates. For the particular mix design studied here, these two aggregate categories are separated at the aggregate size of 2.36 mm. When modeling the asphalt mixture in PF3D, we consider only the coarse aggregates (i.e. aggregate size $\geq$ 2.36 mm) as discrete spheres whereas the bonds between these spheres represent the mixture of asphalt binder and fine aggregates (i.e. FAM). In this way, we can effectively reduce the computational time, which is one of the main obstacles in the application of discrete element models. In the model, the spherical particles are considered to be rigid bodies, and the bonds between these rigid particles are responsible for transmitting both force and moment, which resist the relative motion of the spheres.

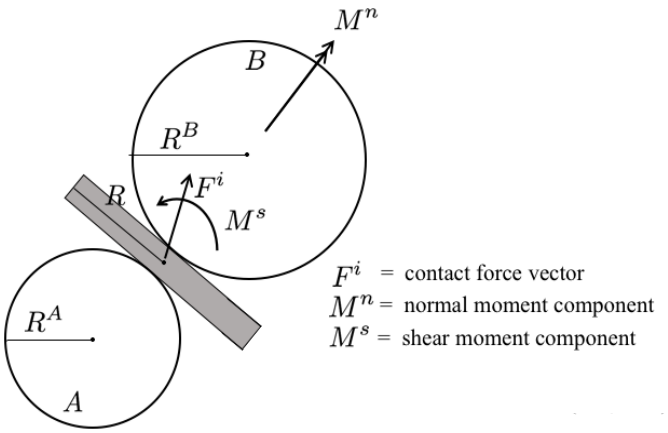

Figure 3.1: Schematic of bond contact forces in the discrete element model.

The inter-particle bond is similar to a set of elastic springs that are uniformly distributed over the cross section on the contact plane (Figure 3.1). The elastic behavior of the bond between the particles contains a set of force and moment relating to the normal and shear components with respect to the contact plane. At each contact surface, the force and moment can be expressed as

$$\vec{F} = F_n\vec{n} + F_s\vec{t} \tag{3-1}$$

$$\vec{M} = M_n\vec{n} + M_s\vec{t} \tag{3-2}$$

where F_n and M_n are the force and moment components in the normal direction, respectively, and F_s and M_s are the force and moment components in the tangential direction, respectively (Figure 3.1). During each time increment of the simulation, the change of these force and moment components are further related to the relative motion of the particles as follows:

$$\Delta F_n = k_n A \Delta\delta_n \tag{3-3}$$

$$\Delta F_s = -k_s A \Delta\delta_s \tag{3-4}$$

$$\Delta M_n = -k_s J \Delta\theta_n \tag{3-5}$$

$$\Delta M_s = -k_n I \Delta\theta_s \tag{3-6}$$

where *A*, *I*, and *J* are the area, moment of inertia, and polar moment of inertia of the bond, respectively. Based on the calculated force and moment, we can determine the maximum normal and shear stresses in the bond based on elastic analysis, i.e.:

$$\sigma_{max} = -F_n/A + |M_s|R/I \tag{3-7}$$

$$\tau_{max} = F_s/A + |M_n|R/J \tag{3-8}$$

where *R* is the bond radius, which is set to equal to the maximum radius of the two particles. As the maximum shear stress exceeds the strength limit, the bond breaks and the force is equal to zero.

As the maximum tensile stress exceeds the strength limit, the bond exhibits softening and the force decreases linearly as the bond length increases until the force is equal to zero. When the force reaches zero, the bond is broken and loses its load-carrying capacity, which indicates that a discrete crack was formed between these two particles. Figure 3.2 shows the constitutive relation of the bond under pure tension, in which T_n denotes the tensile strength of the bond and α is the coefficient of the decreasing slope multiplied by the normal stiffness that produces the required fracture energy of the bond. The fracture energy of the bond is equal to the work of fracture divided by the cross-sectional area. Bond fracture energy is a function of Young modulus and tensile strength and can be calculated as:

$$G_{f,bond} = \frac{W}{A} = \frac{\sigma_{max}^2 L}{2E}\left(1 + \frac{1}{\alpha}\right) \tag{3-9}$$

where α is the coefficient of the softening portion of the slope for the constitutive behavior of the bond and $E = k_n L$ and *L* is the bond length. *L* is set equal to 1 mm since the average diameter of the particles in FAM is approximately 1 mm. Figure 3.3 shows a 3-D representation of the bond between two particles and indicates the bond length and cross-sectional area. The softening parallel-bond model is incorporated into the current PF3D code by modifying its material module.

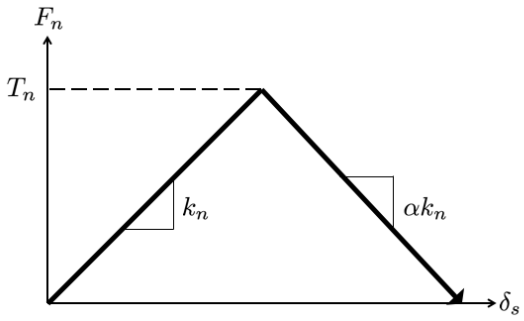

Figure 3.2: Linear parallel-bond model behavior with softening.

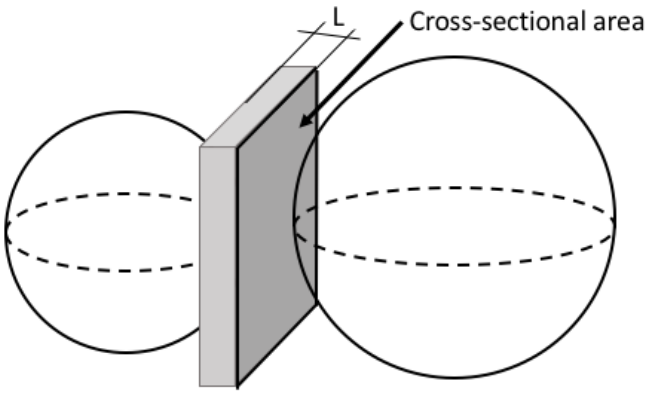

Figure 3.3: Three-dimensional representation of the bond between two particles. The cross-sectional area and bond length are indicated.

3.2 INPUT OF MIXTURE PARAMETERS

The main advantage of the discrete element model is its capability of capturing the details of the microstructures. The present model requires the input of geometry and mixture material properties that include the particle size distribution, the porosity of the particles, the bond gap and radius of the bond. The particle size distribution can be obtained based on the known aggregate size distribution. Note that in this study we only explicitly consider coarse aggregates whereas the fine aggregates are lumped with the binder. For the particular mix design studied, the diameter of the coarse aggregates varies from 2.36 mm to 9.5 mm. The particle size distribution follows that of the asphalt mixture with various percentages passing through each sieve. To incorporate the size distribution information into PFC3D, we determine the particle size intervals for equal intervals of the passing rate (Figure 3.4), from which we generate a smooth particle distribution curve. This is similar to the Latin Hybercube Sampling technique for stochastic simulations [48].

The ratio of void space to the total volume of the larger aggregates that are modeled in the simulation must also be considered. Note that, in the present discrete element model, the porosity of the mixture takes into account both FAM volume and air voids. The various volumes were calculated based on the

material composition, i.e. 52% of the aggregates (by weight of total aggregates) was fine aggregates, and the binder was 5.5% of the total mix (by weight) and the total air voids for the mixture was about 7%. For the mixtures studied here, the porosity was calculated to be approximately 40%.

The parallel bond installation gap and bond radius are shown in Figure 3.1. The gap was determined to be 0.05 mm. This value was chosen so that all particles were bonded to their immediate neighboring particles to simulate aggregates that are completely coated in asphalt binder. The bond radius is equal to the maximum radius of the two particles in contact, which was chosen to model the asphalt binder that surrounds the entire aggregate in the compacted mixture.

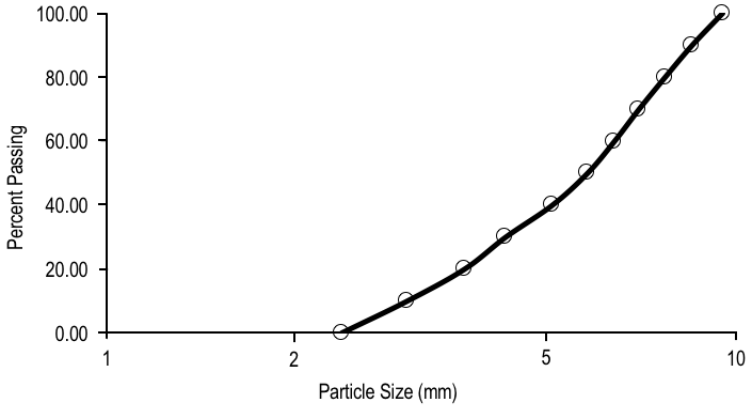

Figure 3.4: Particle distribution curve for coarse aggregates

Based on the aforementioned geometrical parameters, the PFC3D code is used to generate a SCB specimen with a diameter of 150 mm and a thickness of 25 mm, which is used for the experimental investigation. The specimen contains a crack of 3 mm in width and 20 mm in length at the middle of the bottom surface. The SCB specimen is simply supported with a span of 120 mm and is loaded on the top. Figure 3.5 shows one realization of the geometry of the specimen.

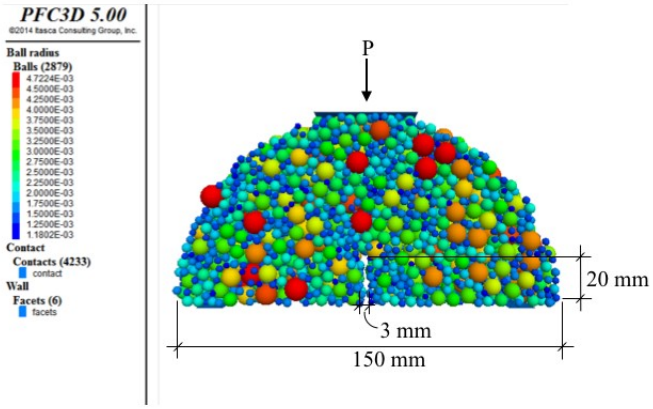

Figure 3.5: Discrete element modeling of semi-circular bend specimen (Ball radius dimensions are shown in meters)

3.3 INPUT OF BOND MATERIAL PROPERTIES

In addition to geometrical parameters, the present model requires six material parameters, which describe the behavior of the bond contact. These parameters include the Young modulus, the Poisson ratio, the tensile strength, the bond fracture energy, the shear strength, and the frictional angle. These parameters are determined as follows:

1) The Young modulus and the tensile strength of the bond are determined from the BBR test (Marasteanu et al. 2012). The test is conducted on compacted samples of asphalt binder and fine aggregates. The fine aggregates used in the FAM had a diameter less than 2.36 mm. The details of the experiments on FAM will be described in the next section.

2) The Poisson ratio υ is considered to be insensitive to temperature, therefore it is taken to be a constant value, 0.3. The stiffness ratio of the bonds, (the normal stiffness divided by the shear stiffness) is calculated from the Poisson ratio, i.e.:

$$k^* = k_n/k_s = E/G = 2(1+\upsilon) \tag{3-10}$$

3) Shear strength is used to model the slip behavior of the bond, which can be considered as mode II fracture. In the simulation of SCB tests, the asphalt mixture primarily experiences tensile cracking (mode I fracture). Therefore, we set a relatively high value of shear strength (20 MPa) so that the bond will primarily fail in tension.

4) Friction angle is important when the specimen experiences compressive failure. This is not the case for SCB specimens. Since the simulation of the SCB test primarily experiences tensile cracking, the friction angle has no effect on the simulation.

5) The fracture energy of the bond is used to determine the slope of the softening part of the linear parallel-bond model behavior. The fracture energy of the bond is the area under the force-displacement curve of the bond divided by the area of the bond (Eq. 3-9). The bond fracture energy is used as a fitting parameter to match the post-peak behavior of the simulation to the experimental results.

Table 3.1 lists both the geometrical properties, mixture material properties, and bond material parameters that are inputted into the PFC3D for the simulations of SCB experiments with unmodified asphalt binder. Table 3.2 lists the material properties of tensile strength, elastic modulus and bond fracture energy for the simulations with various amounts and types of GNP additions. These parameters are discussed further in Section 4.

Table 3.1: Input Parameters for PFC3D

Parameter	**Input**
Porosity	0.4
Bond Gap	0.05 (mm)
Bond Radius	Max(R^1,R^2)
Poisson Ratio	0.3
Bond Fracture Energy	12.64 (J/m^2)
Elastic Modulus	4.29 (GPa)
Tensile Strength	7.05 (MPa)
Cohesion	20 (MPa)
Friction Angle	40^o

Table 3.2: Material input parameters for binder modified with various amounts of GNP

Type of GNP	**M850**	**M850**	**M850**	**4827**	**4827**	**4827**
Amount of GNP added	**0.5%**	**1%**	**3%**	**0.5%**	**1%**	**3%**
Strength (MPa)	9.07	8.27	10.05	10.40	10.26	10.47
Elastic modulus (GPa)	3.87	3.87	4.52	4.81	4.76	3.64
Bond fracture energy (J/m^2)	22.18	18.55	23.19	23.60	22.95	30.59

CHAPTER 4: EXPERIMENTAL INVESTIGATION

This section discusses the procedures and results for the BBR and SCB experiments performed in this research. Section 4.1 discusses the preparation of the specimen for testing. Section 4.2 presents the mixing technique used to mix the GNP and asphalt binder and discusses the benefits of this method. Section 4.3 presents the procedure and results from the BBR tests performed on FAM with various amounts of GNP added. Finally, Section 4.4 discusses the procedure and results from performing the SCB test on asphalt mixtures with various amounts of GNP added.

4.1 DESCRIPTION OF MATERIALS AND PREPARATION OF SPECIMENS

In this study, asphalt mixtures of both modified and unmodified asphalt binder are tested. The unmodified asphalt binder PG 58-34 was obtained from Minnesota Department of Transportation (MnDOT), and manufactured by Flint Hills Resources. The binder was heated for 30 minutes in an oven at 150°C. The binder was then short term aged using a rolling thin film oven (RTFO) in accordance with the AASHTO standard method T240. After short-term aging, a pressurized aging vessel (PAV) was used to accelerate the aging of the mix. This was in accordance with AASHTO Standard method R28-09 and simulates the in-service oxidative aging in the field for an asphalt pavement during 5-7 years of service. After the aging process was finished, the blend was degassed using a vacuum oven and was stored in small cans and reheated to prepare BBR and SCB test samples.

The modified binder samples contained various amounts of graphite nanoplatelets (GNP). Recent studies have shown that the GNP can be easily incorporated into asphalt binders, and due to its relatively low aspect ratio, less potential clustering is observed during the mixing when compared to other nanomaterials. Strength tests showed that GNP modified asphalt binders exhibit superior flexural strength at low temperatures compared to conventional binders. Two different types of GNP were used, 4827 and M850 where type 4827 represents true GNP powder and type M850 is a less expensive GNP flake. The added amount of GNP was 0.5%, 1% and 3% by weight of binder for the modified asphalt binders.

The SCB specimens were prepared by using the mix design provided by the MnDOT. The mixture was prepared using Superpave mix design. The details of the mix design groups are as follows: The mix design is composed of 5.5% binder and three different types of aggregates including, 42% SSG sand, 25% Kraemer 3/8 minus (limestone), and 30% Kraemer 3/8 chip (limestone). The mix design can be found in Table A.1. The compaction was performed using a Brovold Gyratory Compactor. The number of gyrations performed were 60 gyrations. The bulk specific gravity (Gmb) and the maximum specific gravity (Gmm) for the mixture were determined. An air void content of 7.7% was achieved for the compacted specimen.

4.2 MIXING OF GNP INTO ASPHALT BINDER

GNP was mixed with the asphalt binder by using a high shear mixing device. Compared to hand stirring technique, the present mixing technique is more effective at dispersing the GNP into the asphalt binder. A common method for measuring dispersion of nanomaterials through materials is the SEM techniques. However, it cannot be used to measure the dispersion of the GNP into the asphalt binder since the binder and GNP are black in color. Instead, electrical conductivity tests were performed on samples of binder

with various amounts of GNP in order to measure the dispersion of the GNP in the asphalt binder.

A four-probe electrical conductivity test was performed on binder samples with various amounts of GNP. Experiments were performed on unmodified samples and samples with 3% and 6% for both types of GNP, 4827 and M850. The samples were prepared using the high shear mixing device to mix the asphalt and binder. The binder was then poured into molds with dimensions of 6.35 mm thick by 12.70 mm wide and 127 mm long. In the test, four probes were spread out along the sample such that there is an equal distance of material between each probe and the probe set up can be seen in Figure 4.1. The outside probes source the current while the two inside probes sense the voltage drop across the sample. The power supply was 1 volt and the current was 0.0001 micro Amps. Three tests were performed on samples with a given amount and type of GNP.

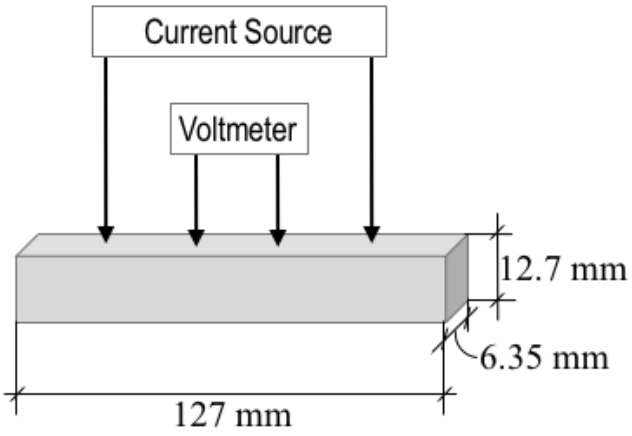

Figure 4.1: Four-point probe setup

The results in Table 4.1 indicate that voltage is measured between the inner probes for the binder samples that contain GNP while no voltage is measured across the unmodified sample. The voltage measured for the samples with various amounts of GNP ranged from 2-4 mV.

Table 4.1: Voltage results from conductivity test on samples of binder with GNP.

GNP Type	4827	4827	M850	M850
Amount of GNP	3%	6%	3%	6%
Voltage (mV)	2.86	3	3.16	3.83

When the same conductivity test was performed on samples of binder mixed with GNP by hand (i.e.

without using the high shear mixing method), no voltage was measured for any of the samples including the samples with 3% or 6% of GNP. Therefore, we may conclude that the high shear mixing technique is more effective at dispersing the GNP throughout the binder.

4.3 BENDING BEAM RHEOMETER TEST ON FINE AGGREGATE MIXTURE SPECIMENS

In order to determine the tensile strength and Young Modulus of the FAM, specimens were prepared for the BBR test. The FAM consists of the fines portion of the mixture with aggregates passing through the No. 8 sieve (2.36 mm). The ignition oven test (AASHTO T308) is used to determine the binder content within the fine aggregate portion of the full mixture [49]. The full mixture requires 5.5% binder, using PG 58-34 binder. The percent binder within the fine aggregate mixture was determined to be 8.7%. This was determined by establishing the aggregate batch size that would be used for the FAM sample and preparing a loose sample of the total mixture. The samples were conditioned for a 2-h period at 135°C. The mixture was passed throw a No. 8 sieve and the parties passing through were oven dried at a temperature of 110°C. The mass of the materials of each group were recorded. The pan was placed in an ignition oven to bur the asphalt in accordance with AASHTO T308. After the binder burning is complete the mass of the pan with materials was recorded. The percent binder was calculated as follows:

$$P_b = \frac{W_M - W_A}{W_M - W_P} \times 100 \qquad (4\text{-}1)$$

Where W_M, W_A, and W_P are the weight of the mixture in pan, materials after binder burning and weight of the pan, respectively.

The BBR test was performed according to [49]. The BBR test system consists of a test frame, a controlled temperature environment, and a computer controlled automated data acquisition component. The sample supports are 3.0 mm in top radius and are at an angle of 45 degrees with the horizontal axis. The supports are made of stainless steel and placed 102 mm apart. The width of the supporting strips is 9.5 mm. The supports also include vertical alignment pins that are 2 to 4 mm in dimeter and are placed at the back of each sample support at 6.75 mm from the center of the support. A blunt-nosed loading shaft with a spherical contact point of 6.35 mm radius is used. A load cell with a minimum capacity of 9.806 mN and having a minimum resolution of 2.5 mN is mounted in-line with the loading shaft to measure contact and test load. A linear variable differential transducer is mounted axially above the loading shaft capable of resolving a linear movement less than 0.15 micrometers with a range of at least 6 mm is used to measure the deflection of the test beam.

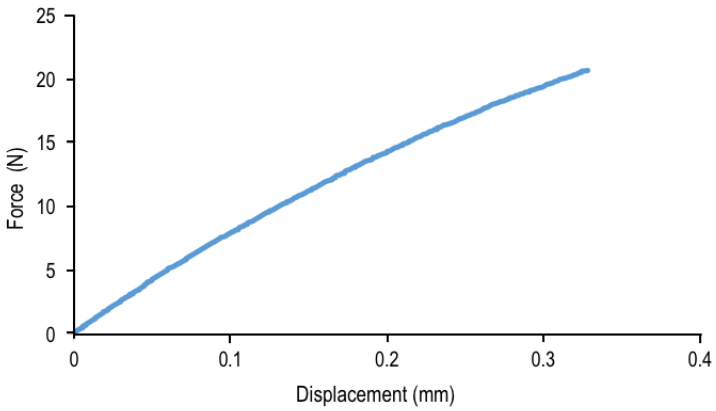

Figure 4.2: Typical force-displacement curve measured in the BBR test.

The FAM was compacted with the same gyratory compactor following the mixture preparation procedure described in the proposed standard test method for preparing dynamic mechanical analyzer specimen [49]. Compacted cylinders of the fine aggregates and binder were prepared and samples were then cut to the dimension of 6.35 mm thick by 12.70 mm wide and 127 mm long. FAM specimens were obtained for unmodified GNP and for each type and percentage of GNP. The thickness and width of each beam were measured in three places and the average was reported for calculation purposes. The BBR strength test was performed on three of each of the FAM specimens at T =24°C, from which the load-deflection curve was recorded. The test was performed by applying a load of 44 N in 150 seconds. Figure 4.2 presents a typical load-deflection curve. From these plots, the maximum load applied and the deflection right before failure are obtained. These values are used to calculate the tensile strength and modulus as follows:

$$E = \frac{P_e L^2}{4bh^3\delta} \tag{4-2}$$

$$\sigma = \frac{3P_m L}{2bh^2} \tag{4-3}$$

where P_m is the maximum load capacity, P_e = 0.5P_m, L, b, h are the length, width and height of the specimen, respectively, and $\delta$is the deflection at which the maximum load is reached. The average tensile strength and modulus were obtained from the three tests on each of the seven FAM. The calculated results for tensile strength and modulus are shown in Table 4.2. The tensile strength for FAM modified with various amounts of GNP show a significant increase of approximately 26% to 42% compared to unmodified FAM. The values obtained for the Young modulus vary from 3.74 GPa to 4.81 GPa.

Table 4.2: Nominal tensile strength and elastic modulus of FAM for unmodified and modified binder

	Amount of GNP Added						
Type of GNP	Unmodified	M850			4827		
	0%	0.5%	1%	3%	0.5%	1%	3%
Tensile Strength (MPa)	6.07	9.07	8.27	10.05	10.40	10.26	10.47
Elastic Modulus (GPa)	4.29	3.87	3.87	4.52	4.81	4.76	3.74

It should be emphasized that the nominal tensile strength calculated from the BBR test does not represent the true tensile strength of the material due to the size effect in quasibrittle fracture. Since it is well known that asphalt mixtures can be considered as a quasibrittle material at low temperatures [51, 52, 53, 54], it is expected that the nominal tensile strength would be subjected to a size effect. By contrast, the value of the Young modulus obtained from the BBR test can directly be inputted into the PF3D since size effect is absent in elasticity [55].

To determine the actual tensile strength of the material, we note that, for geometrically similar beams, the size effect on the nominal tensile strength can be approximated as [55]

$$\sigma_N = T_n \left[\frac{C_1 D_b}{D} + (C_2 D_b / D)^{2r/m} \right]^{1/r} \tag{4-4}$$

where C_1, C_2, and r are constants depending the specimen geometry, m is the Weibull modulus and D_b is the thickness of the boundary layer, which is about four times the average aggregate size [55]. Previous studies have determined the size effect curve represented by Eq. 4-4 for three-point bending of concrete specimen (Fig. 4.3). The Weibull modulus of asphalt mixtures is very close to that of concrete [52]. Therefore, we can use Fig. 4.3 to determine the ratio between the nominal tensile strength and the actual material tensile strength for any given value of D/D_b. In this study, D_b is about 1 mm (average aggregate size is about 0.25 mm) and the depth D_0 of BBR beams is 6.07 mm. Based on Figure 4.3, we have $\sigma_N(D_0) \approx$

$0.85T_n$ or $T_n \approx 7.05$ MPa. Table 4.3 shows all the values of strength after scaling that are inputted into the model.

Table 4.3: Nominal tensile strength of FAM for unmodified and modified binder after scaling

	Amount of GNP Added						
Type of GNP	Unmodified	850			4827		
	0%	0.5%	1%	3%	0.5%	1%	3%
BBR Tensile Strength (MPa)	6.07	9.07	8.27	10.05	10.40	10.26	10.47
Scaled Tensile Strength (MPa)	7.05	10.53	9.60	12.19	12.08	11.92	12.16

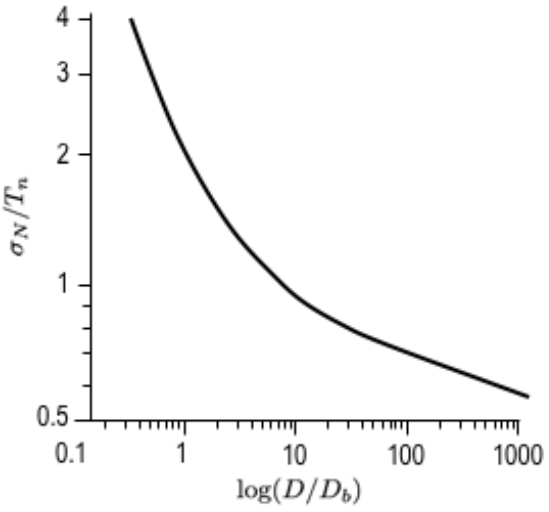

Figure 4.3: Size effect curve for three-point bending of concrete specimen

4.4 SEMI-CIRCULAR BEAM TESTS

In order to investigate the fracture behavior of the asphalt mixtures, we performed the SCB test following AASHTO TP-105 and the measured load-deflection curve is compared with the simulation by PFC3D. The SCB test method takes advantage of the simple specimen preparation from Superpave Gyratory compacted cylinders and the simple loading setup [60]. Figure 4.4 shows the set-up of SCB tests.

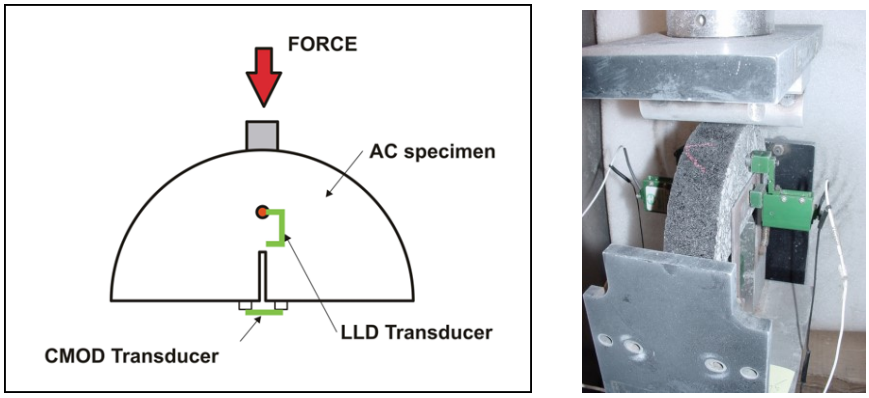

Figure 4.4: Set-up of SCB Tests

In this study, a MTS servo-hydraulic testing system equipped with an environmental chamber was used to perform the SCB test. The SCB samples were symmetrically supported by two fixed rollers and had a span of 120 mm. The load line displacement (LLD) was measured using vertically mounted Epsilon extensometers with 38 mm gage length and ±1 mm range; one end was mounted on a button that was permanently fixed on a specially made frame, and the other end was attached to a metal button glued to the sample. The CMOD was recorded by an Epsilon clip gage with 10 mm gage length and a +2.5 and -1 mm range. The clip gage was attached to the bottom of the specimen. Considering the brittle behavior of asphalt mixtures at low temperatures, the CMOD signal was used as the control signal to maintain the test stability in the post-peak region of the test. A constant CMOD rate of 0.0005 mm/s was used and the load and load-point displacement (*P-u*) curve was plotted. A contact load with maximum load magnitude of 0.3 kN was applied before the actual loading to ensure uniform contact between the loading plate and the specimen. The testing was stopped when the load dropped to 0.5 kN in the post peak region. All tests were performed inside an environmental chamber. Liquid nitrogen was used to obtain the required low temperature. The temperature was controlled by the environmental chamber temperature controller and verified using an independent platinum RTD thermometer. The SCB tests were performed at $T = -24°C$.

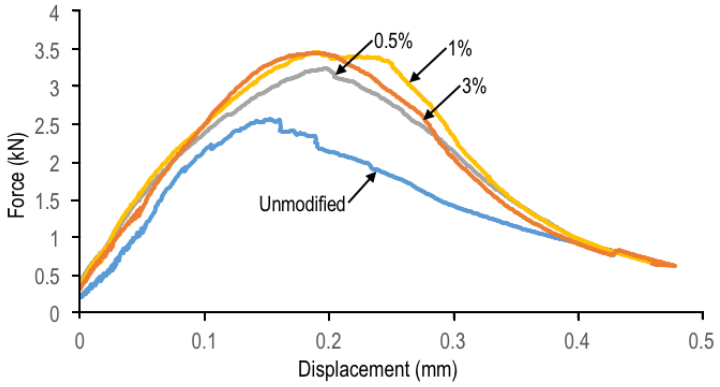

Figure 4.5: Load-deflection curve for asphalt mixtures with unmodified binder and various amounts of GNP M850.

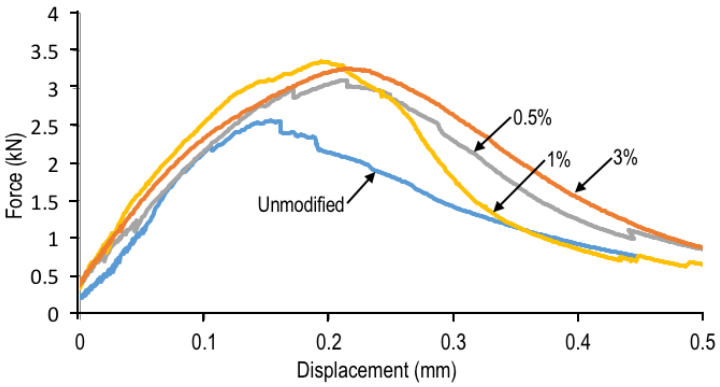

Figure 4.6: Load-deflection curve for asphalt mixtures with unmodified binder and various amounts of GNP 4827.

Figure 4.5 presents the load-deflection curve, which averages the measurements of five specimens for unmodified asphalt binder and binder modified by various amounts of GNP M850. Figure 4.6 presents the average load-deflection curve for mixtures with unmodified binder and GNP 4827. It is clear that the specimens exhibit a gradual softening behavior due to the propagation of the macrocrack, which signifies that the material behaves in a quasibrittle manner. It is well known that the fracture energy of the material can be estimated by dividing the total energy dissipation for crack propagation by the area of newly created crack surface [33]. It is noted from Figs. 4.5 and 4.6 that the measured load-deflection curves do not extend to the point where the load capacity is completely lost. From the experiments, it was observed that at the end of test the remaining ligament length is about 10% of the specimen radius. Therefore, the fracture energy can be estimated as

$$G_f = A_l^{-1}\left(\int_0^{u_0} p\,du - \frac{1}{2}p_0u_0\right) \tag{4-5}$$

where p_0, u_0 = measured load and displacement at the end of test, $A_l = (0.45D - a_0)t$ = total cracking area, *D* = diameter of SCB specimen, *t* = specimen thickness, and a_0 = initial crack length. Note that in Eq. 4-5 the term $0.5p_0u_0$ represents the elastic strain energy stored in the specimen. If the experiments were performed till the complete failure of the specimen (i.e. load capacity drops to zero), the elastic strain energy would vanish.

As seen from Figs. 4.5 and 4.6, the fracture energy of GNP modified asphalt mixtures is significantly greater than the unmodified binder mixtures, an increase ranging from 18% to 27% (as listed in Table 4.4). The peak load capacity of the asphalt mixtures also shows a significant increase for asphalt binder modified with GNP compared to unmodified binder with an increase of approximately 18% to 26%. These results indicate that GNP can effectively improve the fracture behavior of asphalt mixtures at low temperatures.

Table 4.4: Fracture energy of the asphalt specimen from the SCB test

Type of GNP	Unmodified	M850	M850	M850	4827	4827	4827
Amount added	0%	0.5%	1%	3%	0.5%	1%	3%
Fracture Energy (J/m^2)	471.1	640.5	741.4	723.7	712.6	698	870.3

CHAPTER 5: RESULTS AND DISCUSSION

Section 5.1 presents the discussion of the comparison between the simulation and experimental results. A parametric study is also presented in section 5.2 exploring how the bond behavior would affect the overall mechanical response of the asphalt mixtures. The results of the parametric study can be used a design tool for asphalt pavements with various amounts of GNP. The required tensile strength of the pavement for target fracture behavior can be determined using the results from the parametric study.

5.1 COMPARISON OF DEM AND EXPERIMENTAL MEASUREMENTS

The discrete element model was used to simulate the aforementioned SCB experiments on both conventional and GNP modified asphalt mixtures. For each material, the measured elastic modulus and tensile strength of FAM were inputted into the constitutive model of the bond contact (Fig. 3.2). The fracture energy of the bond (Eq. 3-9) is the only model parameter that was fitted. In the discrete element simulations, for each SCB specimen 10 realizations of the random microstructure (i.e. random particle size and placement) were used to obtain an average response. The fracture energy of the bond was estimated by minimizing the difference between the simulation and experimental results.

Figure 5.1 presents the comparisons between the experiment measurement and simulation results for conventional asphalt mixtures. Here two types of bond contact behavior were considered: 1) a softening bond contact law (Fig. 3.2), i.e. α has a finite value, and 2) a perfectly brittle bond contact law, in which the load capacity of the bond suddenly drops to zero once the peak strength is reached, i.e. $\alpha \to \infty$. Both models have the same initial elastic modulus and peak strength. Based on Fig. 5.1, it can be seen that the post-peak behavior of the bond contact (i.e. FAM) has a dominant influence on the post-peak behavior of the load-deflection curve of the mixtures. This implies that it is necessary to employ a softening bond contact law in order to determine the fracture energy of mixtures. However, the elastic response and the peak load capacity of the SCB specimens are affected mildly by the post-peak response of the FAM. It should be noted that the degree of the influence of post-peak response of FAM on the peak load capacity of mixture specimens also depends on the specimen size. For small-size mixture specimens, the failure is quasi-plastic, for which the peak load capacity is primarily governed by the strength of the bond contact. By contrast, large-size mixture specimens exhibit a perfect brittle failure mode, for which the peak load capacity will be governed primarily by the fracture energy of the bond contact. Therefore, it is necessary to employ a realistic softening constitutive model for the bond contact (FAM) for the discrete element model of the asphalt mixtures.

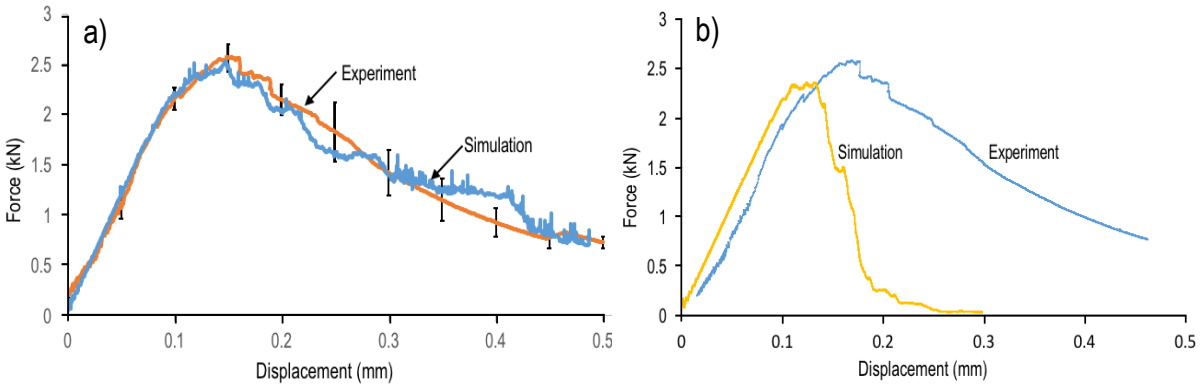

Figure 5.1: Comparison between the simulated and measured load-displacement curves of conventional asphalt mixture specimens: a) with calibrated fracture energy of the bond contact, and b) with a perfectly brittle bond contact.

Figure 5.2 presents the results for the SCB experimental measurements and the simulation results for the GNP modified asphalt mixtures. The experimental result of each mix represents the average of the five tests, and the scatter of the five tests is shown as the error bar. In this analysis, the simulations used a softening bond contact model and the input fracture energy of the bond was calibrated to fit the experimentally measured load-displacement curve. It is seen that the computational model can match the experimental results reasonably well in terms of the elastic response, the peak load capacity, as well as the post-peak softening.

It is found that the measured load-displacement curves have a non-zero starting force, which is due to instances where data recording starts at a load value different from zero. However, the simulated displacement at which the peak load occurs is in agreement with the experimental results. Meanwhile, it is observed that, compared to the experimental results, the numerical simulations tended to predict a steeper descending slope right after the peak load. This could be attributed to the nature of the discrete element model. In the discrete element model, there are a limited number of particles (coarse aggregates) along the uncracked ligament. The crack propagation is presented by the breakage of a small number of connections (contact bonds). As a result, the stress profile in the simulated specimen is not continuous, and each breakage is manifested by a drop of load capacity. In the actual specimens, the crack propagates in a continuous medium. If the specimen size is sufficiently large, the average response predicted by the discrete element model should converge to the experimental results. The other possible reason for the discrepancy is that we adopted a linear softening behavior for the FAM while the actual softening law could be more complicated.

Nevertheless, it should be pointed out that, for all types of mixtures, the area under the simulated force-displacement curve compares well with the experimental observation. Table 5.1 presents the input fracture energy of the bond contact and the fracture energy of the mixtures inferred from the experiments. It is seen that these two fracture energies differ by an order of magnitude. This indicates that the macrocrack growth in the SCB specimens must be associated with a finite size of fracture process zone. The formation of the fracture process zone consists of breakage and partial damage of many bond contacts. The fracture energy of the mixtures is governed by the weighted sum of the energy dissipations of these bond contacts, which include dissipation due to fracture and damage as well as elastic energy dissipation in shear. It is the area under the softening law of the FAM (fracture energy of the bond contact)

that is crucial for predicting the fracture energy of the mixture specimens. Therefore, even with a simple softening law is used for FAM, the model is able to capture correctly the overall fracture energy of the mixtures.

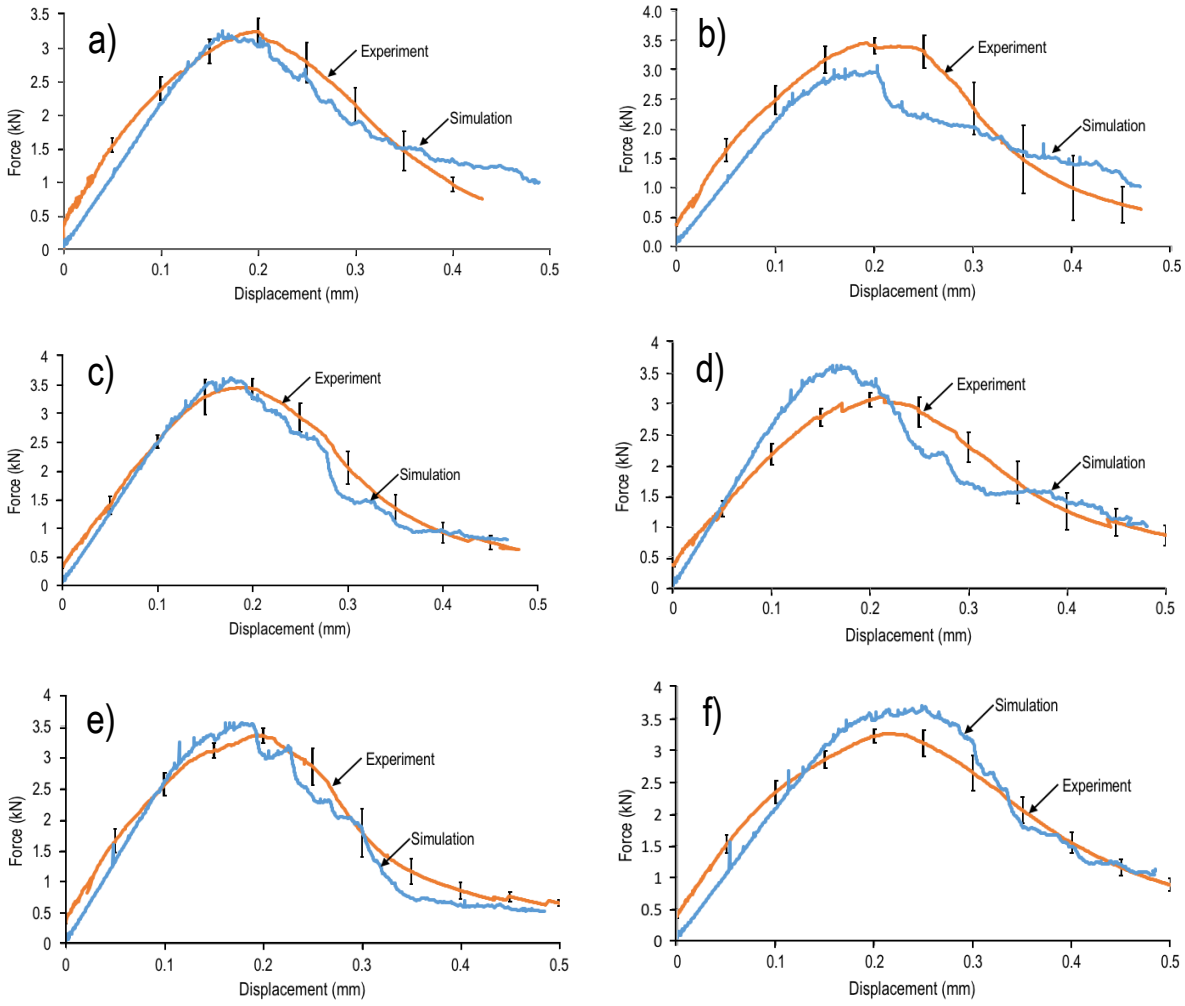

Figure 5.2: Comparison between the simulated and measured load-displacement curves of GNP modified asphalt mixture specimens: a) 0.5% GNP M850, c) 3% GNP M850, d) 0.5% GNP 4827, e) 1% GNP 4827, and f) 3% GNP 4827.

Table 5.1 Fracture energy of the asphalt specimen measured from the SCB test

	Amount of GNP Added						
Type of GNP	None	850			4827		
	0%	0.5%	1%	3%	0.5%	1%	3%
Input fracture energy of bond (N/m)	12.64	22.18	18.55	23.19	23.60	22.95	30.59
Measured fracture energy of mixtures (N/m)	471.1	640.5	741.4	723.7	712.6	698	870.3

It is noted that in the present analysis we adopted a size effect model (Eq. 4-4) to scale the BBR strength as an input of the strength of bond contact. To demonstrate the role of this scaling procedure, Figure 5.3 shows the simulated load-deflection responses of the conventional asphalt mixtures with and without scaling the BBR strength. It is found that, without scaling the tensile strength, the elastic response is in good agreement with the SCB results but the peak load capacity predicted by the numerical model is considerably lower (about 20%) than that obtained from the SCB test. The discrepancy of the predicted load capacity is approximately the same as the level of adjustment of the strength of bond contact by considering the size effect. This also supports the aforementioned discussion on the dominant influence of the bond strength on the peak load capacity of the mixtures. Therefore, we may conclude that the scaling procedure is necessary for predicting the load capacity of the SCB specimens.

It is admitted that, in the present analysis, the bond fracture energy is a fitting parameter and therefore the discrete element model is not fully predictive. However, the present results show several promising features of the model, which indicate the possibility that the fracture behavior of the mixtures could be predicted by the fracture properties of FAM. The current BBR test can only measure the load-displacement curve up to the peak load, which can be used to calculate the elastic modulus and the material tensile strength of the FAM. Following are several practical methods that could be used to determine the fracture energy of FAM:

1) One could perform fracture tests (e.g. SCB or DCT tests) on FAM, from which the fracture energy can be calculated based on the work-of-fracture method [33]. The fracture energy can then be used to determine the total energy dissipation of the bond.

2) One could perform the BBR tests on FAM specimens of different depths. The measured size effect on the nominal tensile strength of the FAM specimens can be used to determine the fracture energy, and therefore the total energy dissipation of the bond [55]. It should be noted that, compared to the fracture tests, the size effect tests are simpler because they do not need enter the post-peak regime, though they will require more specimens.
3) One could perform the BBR tests on notched FAM specimens of different notch depths. Through the analysis of the effect of notch depth on the peak load capacity, one can determine the fracture energy and tensile strength of the FAM [55].

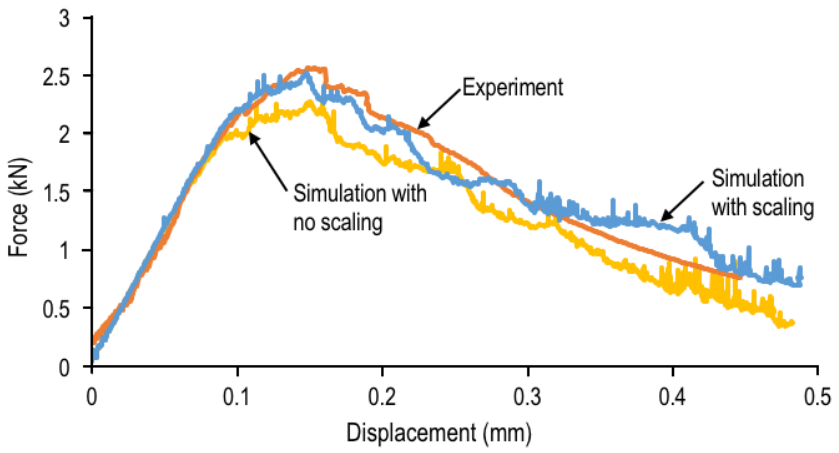

Figure 5.3: Effect of scaling of bond strength on the computed load-displacement curves for conventional asphalt mixtures.

5.2 PARAMETRIC STUDY

A parametric study is performed to gain understanding of how the bond behavior would affect the overall mechanical response of the mixtures. The motivations for understanding the relationship between the bond behavior and mixture behavior are twofold: 1) it will allow us to design appropriate laboratory experiments on FAM in order to predict the mixture behavior, and 2) it will help us propose new mix designs to achieve certain desirable behavior of the mixtures. The present parametric study investigates three key model parameters, i.e. the elastic modulus, tensile strength and bond fracture energy. The bond fracture energy is a function of elastic modulus, tensile strength and parameter α, which is used to determine the decreasing slope of the softening behavior of the constitutive relationship describing the

bond.

The fracture energy of the mixtures is a function of the tensile strength, elastic modulus and bond fracture energy of FAM as well as the bond length as shown:

$$G_f = \Pi\left(T, E, G_{f,bond}, L\right) \tag{5-1}$$

According to the Buckingham-∏ theorem (56, 57, 58), Eq. 11 can be rewritten in a dimensionless form as

$$G_f/EL = \Phi\left(T/E, G_{f,bond}/TL\right) \tag{5-2}$$

Based on the simple softening law adopted for the bond contact, the bond fracture energy can be further expressed as a function of the elastic modulus, tensile strength, and value of α:

$$G_{f,bond}/LT = \frac{T}{2E}\left(1 + \frac{1}{\alpha}\right) = \gamma\frac{T}{E} \tag{5-3}$$

where $\gamma = 0.5\left(1 + \frac{1}{\alpha}\right)$ and is a constant for a given mixture. Therefore, for a given α value, Eq. 5-2 can be simplified as

$$G_f/EL = \Phi_1(T/E) \tag{5-4}$$

As a demonstration, we performed a parametric study on the conventional asphalt mixtures by changing the tensile strength of the bond contact. In the analysis, we kept the parameter $\boldsymbol{\alpha}$ constant ($\boldsymbol{\alpha = 0.845}$), which implies that the fracture energy of the bond contact would change in proportion to the bond tensile strength. For each value of the tensile strength, we calculated the fracture energy of the mixture by dividing the area under the simulated load-deflection curve by the original ligament area. Figure 5.4 presents the simulated relationship between the dimensionless parameters $\boldsymbol{G_f/EL}$ and $\boldsymbol{T/E}$. It is seen that, over the practical range of $\boldsymbol{T/E}$ values, the dimensionless parameters $\boldsymbol{G_f/EL}$ and $\boldsymbol{T/E}$ can be reasonably approximated by a linear relationship.

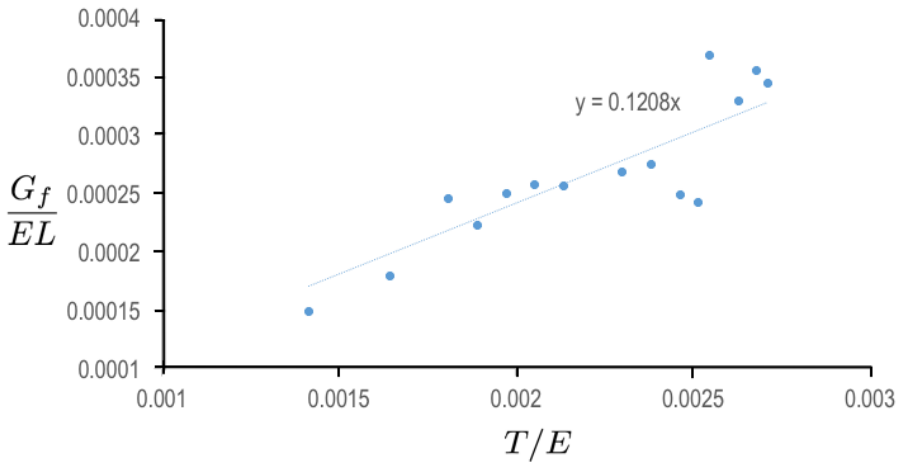

Figure 5.4: Simulated relationship between dimensionless parameters G_f/EL and T/E

Using the linear relationship presented in Fig. 5.4, we can determine the tensile strength of FAM to achieve a target value of fracture energy of the mixtures. This method can also be applied to GNP modified asphalt mixtures. Table 5.2 presents the values of parameter α for GNP modified asphalt mixtures, which were calculated from calibrated fracture energy of the bond contact. It is seen that the amount of GNP addition does not change the parameter α. Therefore, we may re-construct Fig. 5.4 for GNP modified asphalt mixtures, which should be applicable to different amount of GNP additions. Based on the relationship between parameters G_f/EL and T/E, we can determine the tensile strength of GNP modified FAM for the required fracture energy of the mixtures. BBR tests can be performed on FAM to determine the amount of GNP needed to achieve the required tensile strength.

Table 5.2 Values of α used to determine the required bond fracture energy to fit the simulation to the experimental results

	Amount of GNP Added						
Type of GNP	None	850			4827		
	0%	0.5%	1%	3%	0.5%	1%	3%
α value	0.845	0.92	0.91	0.93	0.91	0.93	0.92

CHAPTER 6: CONCLUSIONS AND DISCUSSION

This research investigates the application of a discrete element computational model for predicting the peak load and post-peak behavior for the fracture behavior of asphalt mixtures at low temperatures. The findings of the study can be summarized as follows:

1.) The use of GNP in asphalt binder exhibits significant improvements in strength and fracture energy when compared to unmodified asphalt binder.

2.) High shear mixing technique allows a better dispersion of GNP in asphalt binders and yields higher strength and fracture energy of the mixtures.

3.) The elastic modulus can be obtained by performing the BBR test on FAM, and it can be directly input into the discrete element model to predict the elastic response of the mixture.

4.) The tensile strength of the bond contact of the discrete element model can be obtained from the BBR test result with the size effect adjustment. It is shown that the discrete element model is capable of predicting the peak load capacity of the mixture specimens.

5.) The analysis of the size effect on the tensile strength of the simulation shows that the peak load capacity is governed by the bond strength.

6.) The results of the parametric study indicate that the discrete element model could be used as a design tool to determine the percentage of GNP that is needed to achieve the necessary bond tensile strength for a target fracture energy of the mixtures.

7.) The post-peak softening response can be captured by employing a softening curve for the bond behavior, which requires the input of the bond fracture energy. To obtain the energy needed to fracture the bond, more sophisticated experiments on FAM would be required.

REFERENCES

[1] Hou, Y., Wang, L., Yue, P., Pauli, T., & Sun, W. (2014). Modeling mode I cracking failure in asphalt binder by using nonconserved phase-field model. *Journal of Materials in Civil Engineering, 26*(4), 684–691.

[2] Wang, D., Wang, L., Gu, X., & Zhou, G. (2013). Effect of basalt fiber on the asphalt binder and mastic at low temperature. *Journal of Materials in Civil Engineering, 25*(3), 355–364.

[3] Yang, J., & Tighe, S. (2013). A Review of Advances of Nanotechnology in Asphalt Mixtures. *Procedia - Social and Behavioral Sciences, 96,* 1269–1276.

[4] Gu, X., Xu, T., & Ni, F. (2014). Rheological behavior of basalt fiber reinforced asphalt mastic. *Journal of Wuhan University of Technology-Mater. Sci. Ed., 29*(5), 950–955.

[5] Hossain, Z., Zaman, M., Saha, M., & Hawa, T. (2014). Evaluation of viscosity and rutting properties of nanoclay-modified asphalt binders. *Geo-Congress 2014 Technical Papers*, *GSP 234*, 3695–3702.

[6] Arabani, M., & Faramarzi, M. (2015). Characterization of CNTs-modified HMA's mechanical properties. *Construction and Building Materials, 83*, 207–215.

[7] Yan, Y., Cocconcelli, C., Roque, R., Nash, T., Zou, J., Hernando, D., & Lopp, G. (2015). Performance evaluation of alternative polymer-modified asphalt binders. *Road Materials and Pavement Design*, *16,* 389-403.

[8] Nanoclays. (n.d.). Retrieved July 31, 2015, http://www.sigmaaldrich.com/materials-science/nanomaterials/nanoclay- building.html

[9] Yao, H., Li, L., Xie, H., Dan, H., & Yang, X. (2011). Microstructure and performance analysis of nanomaterials modified asphalt. *Geotechnical Special Publication No. 223: Road Materials and New Innovations in Pavement Engineering,* 220-228.

[10] Jahromi S., & Ghaffarpour, K.A. (2009). Effects of nanoclay on rheological properties of bitumen binder. *Construction and Building Materials, 23*, 2894-2904.

[11] Zare-Shahabadi, A., Shokuhfar, A., & Ebrahimi-Nejad, S. (2010). Preparation and rheological characterization of asphalt binders reinforced with layered silicate nanoparticles. *Construction and Building Materials, 24*(7), 1239-1244.

[12] Nazzal, M., Kaya, S., Gunay, T., & Ahmedzade, P. (2013). Fundamental characterization of asphalt clay nanocomposites. *Journal of Nanomechanics and Micromechanics J. Nanomech. Micromech., 3*(1), 1-8.

[13] Abdelrahman, M., Katti, D., Ghavibazoo, A., Upadhyay, H., & Katti, K. (2014). Engineering physical

properties of asphalt binders through nanoclay asphalt Interactions. *J. Mater. Civ. Eng. Journal of Materials in Civil Engineering, 26* (12), 04014099

[14] Mun, S., & Lee, H. (2011). Modeling viscoelastic crack growth in hot-mix asphalt concrete mixtures using a disk-shaped compact tension test. *J. Eng. Mech., 137*(6), 431-438.

[15] Barik, T. K., Sahu, B, & Swain, V. (2008) Nanosilica-from medicine to pest control Parasitol. *Parisitol Res, 103*, 253-258.

[16] Yao, H., You, Z., Li, L., Lee, C. H., Wingard, D., Yap, Y. K., Shi, X., & Goh, S. W. (2013). Rheological properties and chemical bonding of asphalt modified with nanosilica. *J. Mater. Civ. Eng. Journal of Materials in Civil Engineering, 25*(11), 1619-1630.

[17] Yusof, N., Breem, A., Alattug, H., Hamim, A., & Ahmad, J. (2014). The effects of moisture susceptibility and aging conditions on nano-silica/polymer-modified asphalt mixtures. *Construction and Building Materials, 72*, 139-147.

[18] Al-Adham, K., & Arifuzzaman, M. (2014). Moisture damage evaluation in carbon nanotubes reinforced asphalts. *In book: Sustainability, Eco-efficiency, and Conservation in Transportation Infrastructure Asset Management*, 103-109.

[19] Shirakawa, T., Tada, A. & Okazaki, N. (2012). Development of functional carbon nanotubes-asphalt composites. *International Journal of GEOMATE, 2*(1), 161- 165.

[20] Basalt Fiber Properties, Advantages and Disadvantages. (n.d.). Retrieved July 31, 2015. http://www.build-on-prince.com/basalt-fiber.html#sthash.1bkllF7E.dpbs

[21] Zheng, Y., Cai, Y., Zhang, G., & Fang, H. (2014). Fatigue property of basalt fiber-modified asphalt mixture under complicated environment. *Journal of Wuhan University of Technology-Mater. Sci. Ed., 29*(5), 996-1004.

[22] Gao, C., Han, S., Chen, S., & Li, H. (2014). Research on basalt fiber asphalt concrete's low temperature performance. *AMM Applied Mechanics and Materials*, *Vol. 505-506*, 35-38.

[23] Novoselov, K.S., Geim, A.K., Morozov, S.V., Jiang, D., Katsnelson, M.I., Grigorieva, I.V., Dubonos, S.V., & Firsov, A.A. (2005) Two-dimensional gas of massless Dirac fermions in graphene. *Nature, 438*, 197.

[24] Zhang, Y., Tan, Y. W., Stormer, H. L., & Kim, P. (2005) Experimental observation of the quantum Hall effect and Berry's phase in graphene. *Nature, 438*, 201.

[25] Lee, C., Wei, X., Kysar, J. W., & Hone, J. (2008) Measurement of the elastic properties and intrinsic strength of monolayer graphene. *Science, 321*, 385.

[26] Kim, K., Regan, W., Geng, B., Aleman, B., Kessler, B. M., Wang, F., Crommie, M. F., & Zettl, A. (2010) High-temperature stability of suspended single-layer graphene. *Phys. Status Solidi, RRL4, 11*, 302-304.

[27] Kim, Y., Allen, D., & Little, D. (2005). Damage-induced modeling of asphalt mixtures through computational micromechanics and cohesive zone fracture. *J. Mater. Civ. Eng. Journal of Materials in Civil Engineering, 17*(5), 477–484.

[28] Arago, F., & Kim, Y. (2010) Modeling fracture and failure of heterogeneous and inelastic asphaltic materials using the cohesive zone concept and the finite element method. *GeoFlorida 2010,* 2662–2671.

[29] Huang, H., Lecampion, B., & Detournay, E. (2012). Discrete element modeling of tool-rock interaction I: Rock cutting. *International Journal for Numerical and Analytical Methods in Geomechanics, 37,* 1913-1929.

[30] Ban, H., Kim, Y., & Rhee, S. (2012). Computational microstructure modeling to estimate progressive moisture damage behavior of asphaltic paving mixtures*. International Journal for Numerical and Analytical Methods in Geomechanics, 37*(13), 2005-2020.

[31] Dugdale, D.S. (1960). Yielding of steel sheets continuity slits. *J. Mech. Phys. Solids, 8*(2), 100-104.

[32] Barrenblatt, G.I. (1959). The mathematical theory of equilibrium of cracks in brittle fracture. *Adv. Appl. Mech., 7*, 55-129.

[33] Bazant, Z. P. & Planas, J. (1998). Fracture and size effect in concrete and other quasibrittle materials. *Boca Raton and London: CRC Press.*

[34] Im, S., Ban, H., & Kim, Y. (2014). Rutting and cracking modeling of asphalt pavements considering nonlinear viscoelasticity and cohesive zone fracture. *Asphalt Pavements*, 775-783.

[35] Schillinger, D., Borden, M.J., & Stolarski, H.K. (2015). Isogeometric collocation for phase-field fracture models. *Computer Methods in Applied Mechanics and Engineering, 284*, 583-610.

[36] Borden, M.J., Verhoosel, C.V., Scott, M.A., Hughes, T.J.R., & Landis, C.M. (2012). A phase-field description of dynamic brittle fracture. *Computer Methods in Applied Mechanics and Engineering*, 217-220,77-95.

[37] Cusatis, G., Baant, Z. P. & Cedolin, L. (2003). Confinement-shear lattice model for concrete damage in tension and compression: I. Theory. *Journal of Engineering Mechanics ASCE, 129*(12), 1439–1448.

[38] Cusatis, G., Baant, Z. P. & Cedolin, L. (2003). Confinement-shear lattice model for concrete damage in tension and compression: II. Computation and validation. *J. Eng. Mech. Journal of Engineering Mechanics, 129*(12), 1449-1458.

[39] Cundall, P.A. & Strack, O. D. L. (1979). A discrete numerical model for granular assemblies. *Geotechnique, 29*, 47–65.

[40] Liliu, G., & van Mier, J. G. M. (2003). 3d lattice type fracture model for concrete. *Engineering Fracture Mechanics, 70*, 927–941.

[41] Schauffert, E. A. & Cusatis, G. (2011). Lattice discrete particle model for fiber-reinforced concrete. I: *Theory. Journal of Engineering Mechanics ASCE, 138*(7), 826–833.

[42] Zubelewicz, A. & Bazant, Z. P. (1987). Interface modeling of fracture in aggregate composites. *Journal of Engineering Mechanics ASCE, 113*(11), 1619–1630.

[43] Abbas, A., Papagiannakis, A., & Masad, E. (2005). Micromechanical simulation of asphaltic materials using the discrete element method. *In Proceedings: R. Lytton Symposium on Mechanics of Pavements,*, 1–11.

[44] Hyunwook, K., & Buttlar, W. G. (2009). Discrete fracture modeling of asphalt concrete. *International Journal of Solids and Structures, 46*(13), 2593–604.

[45] Aragao, F., Kim, Y., Lee, J., & Allen, D. (2011) Micromechanical model for heterogeneous asphalt concrete mixtures subjected to fracture failure. *Journal of Materials in Civil Engineering, 23*(1), 30–38.

[46] Potyondy, D. (June 23, 2016). Material-Modeling Support in PFC [via fistPkg23]. Technical Memorandum ICG7766-L, Itasca Consulting Group, Inc. Minneapolis, MN.

[47] Potyondy, D. O., & Cundall. P. A. (2004). A Bonded-particle Model for Rock. *International Journal of Rock Mechanics and Mining Sciences, 41* (8), 1329–1364.

[48] Bazant, Z. P., Vorechovsky, M., & Novak, D. (2007). Energetic-statistical size effect simulated by SFEM with stratified sampling and crack band model. *International Journal for Numerical Methods in Engineering, 71*, 1297–1320.

[49] Marasteanu M., Cannone Falchetto, A., Turos, M., & Le, J.-L. (2012). Development of a simple test to determine the low temperature strength of asphalt mixtures and binders. NCHRP-IDEA Program Project Final Report, National Academy of Sciences, Washington D.C.

[50] Sousa, P., Kassem, E., Masad, E., & Little, D. (2013). New design method of fine aggregate mixtures and automated method for analysis of dynamic mechanical characterization data. *Journal of Construction and Building Materials, 41*, 216– 223.

[51] Cannone Falchetto, A., Le, J.-L., Turos, M.I., & Marasteanu, M.O., (2014) Indirect determination of size effect on strength of asphalt mixture at low temperatures. *Materials and Structures*, Vol. 47 (1-2), 2014, pp. 157–169.

[52] Le, J.-L., Cannone Falchetto, A., & Marasteanu, M.O. (2013), Determination of strength distribution of quasibrittle structures from size effect analysis. *Mechanics of Materials*, Vol *66*, pp. 79–87.

[53] Li, X., & Marasteanu, M. O. (2010) The fracture process zone in asphalt mixture at low temperature. *Engineering Fracture Mechanics,* Vol 77, 1175–1190.

[54] Zegeye, E., Le, J.-L., Turos, M. & Marasteanu, M.O. (2012), Investigation of size effect in asphalt mixture fracture testing at low temperature. *Road Materials and Pavement Design,* Vol *13*, pp. 88–101.

[55] Bažant, Z. P. (2005) *Scaling of structural strength*. London: Elsevier.

[56] Buckingham, E. (1914) On physically linear systems; illustration of the use of dimensional equations. *Phys. Rev. Ser. 2(4)*, 345–376.

[57] Buckingham, E. (1915) Model experiments and the form of empirical equations. *Trans. ASM*E, *37*, 263–296.

[58] Barenblatt, G.I. (1996) *Scaling, Self-Similarity, and Intermediate Asymptotics.* Cambridge: Cambridge University Press.

APPENDIX A: ASPHALT MIX DESIGN

Table A.1: Asphalt Mix Design

Sieve Size (mm)	Composite Formula
25.0	
19.0	
12.5	
9.5	100
4.75	69
2.36	52
1.18	43
0.6	27
0.3	14
0.15	8
0.075	4.7
Spec.Voids	**4.0**
%AC	**5.5**